DOI 10.1007/s00198-009-0868-3

Diffraction techniques and vibrational spectroscopy opportunities to characterise bones

D. Bazin · C. Chappard · C. Combes · X. Carpentier · S. Rouzière · G. André · G. Matzen · M. Allix · D. Thiaudière · S. Reguer · P. Jungers · M. Daudon

Introduction

From a histological point of view, bones that allow body mobility and protection of internal organs consist not only of different organic and inorganic tissues but include vascular and nervous elements as well. Moreover, due to its ability to host different ions and cations, its mineral part represents an important reservoir, playing a key role in the metabolic activity of the organism. From a structural point of view, bones can be considered as a composite material displaying a hierarchical structure at different scales [1, 2]. At the nanometre scale, an organic part, i.e. collagen fibrils and an inorganic part, i.e. calcium phosphate nanocrystals [3, 4] are intimately mixed to assure particular mechanical properties.

A detailed understanding of the correlation between the mechanical properties and structural characteristic of bone has long been a prime concern of the medical community. Among the techniques often used to characterise such biological samples, diffraction techniques (using neutrons, X-rays or electrons as probes) [5] and vibrational spectroscopy (including Raman and Fourier transform infrared (FT-IR) spectroscopy) [6, 7] constitute two families very effective to study mineralised tissues. Recent experimental developments

D. Bazin (✉) · S. Rouzière
Laboratoire de Physique des Solides, Bat 510, Université Paris XI,
91405 Orsay, France
e-mail: Bazin@lps.u-psud.fr

C. Chappard
Equipe Inserm 658, Hôpital Porte Madeleine,
BP 2439, 45032 Orléans Cedex 1, France

C. Combes
CIRIMAT-ENSIACET,
118 Route de Narbonne,
31077 Toulouse Cedex 04, France

X. Carpentier
Service d'Urologie, AP-HP, Hôpital Tenon,
1 Rue de la Chine,
75743 Paris Cedex 15, France

G. André
Laboratoire Léon Brillouin, (CEA-CNRS) Saclay,
91191, Gif-sur-Yvette Cedex, France

G. Matzen · M. Allix
CEMHTI,
1D avenue de la Recherche Scientifique,
45071 Orléans Cedex 2, France

D. Thiaudière · S. Reguer
Synchrotron SOLEIL,
L'Orme des Merisiers Saint-Aubin,
BP 48, 91192 Gif sur Yvette, France

P. Jungers
Service de Nèphrologie,
AP-HP, Hôpital Necker-Enfants Malades, Service de Nèphrologie,
149 Rue de Sèvres,
75743 Paris Cedex 15, France

M. Daudon
Lab. de Biochimie A,
AP-HP, Hôpital Necker-Enfants Malades,
149 Rue de Sèvres,
75743 Paris Cedex 15,
France

permit now in vivo experiments at the micrometre scale [8, 9]. The literature upon diffraction techniques and Raman spectroscopy is large, and numerous excellent review papers and books exist in which the physics associated with and specific experimental devices are described in detail [10, 11]. Thus, we will just present some salient points regarding wide angle X-ray scattering (WAXS), powder neutron diffraction (PND), and Raman spectroscopy quite important when bones are the subject of interest. In order to discuss the advantages and the limits of these techniques, the starting point is given by a simplified structural description of the mineral part of bones at the nanometre scale.

Bone at the nanometre scale

Biological apatites are usually described as substituted calcium hydroxyapatite (HAP, $Ca_{10}(PO_4)_6(OH)_2$). The most common ion substitutions consist in the replacement of the original constituting ions, namely Ca^{2+}, PO_4^{3-} and OH^-, with ions possessing the same electric charge (for example F^- substituted for OH^-) and structure. The second type of substitution consists in the replacement of the original ions by ions with different charges (for example CO_3^{2-} substituted for PO_4^{3-} and/or OH^-) and/or structure. This type of substitution needs a charge compensation mechanism which seems particularly adaptable in apatites due to the possibilities of ion insertions and ion vacancies. Apatitic calcium phosphates offer a wide range of ion substitutions which can modify the physical–chemical and biological properties of apatites. The apatite prototype structure was first determined by Naray-Szabo [12]. Since that pioneer work, there has been a substantial number of researches dedicated to apatites which are conventionally regarded as conforming to $A_5(BO_4)_3X$ general chemical formula [13]. Quite surprisingly, a first difficulty emerges from the lack of OH^- as noticed through several studies based on infrared spectroscopy and inelastic neutron scattering [14, 15]. Thus, in order to estimate the hydroxyl ion content of the calcium phosphate crystals, Cho et al. [16] have taken full advantages of solid-state nuclear magnetic resonance spectroscopy to measure an OH^- content of human cortical bone of about 20% of the amount expected in stoichiometric HAP.

As previously indicated, the crystals of apatite present inside bones are nanometre-sized. Using a transmission electron microscope (TEM), needle-like morphologies [17] are visualised (Fig. 1).

This small size is a crucial factor related to the solubility of biological apatites when compared with geological apatites. Also, alterations of these structural characteristics have been viewed as a consequence of major pathologies such as osteoporosis (see for example [18]).

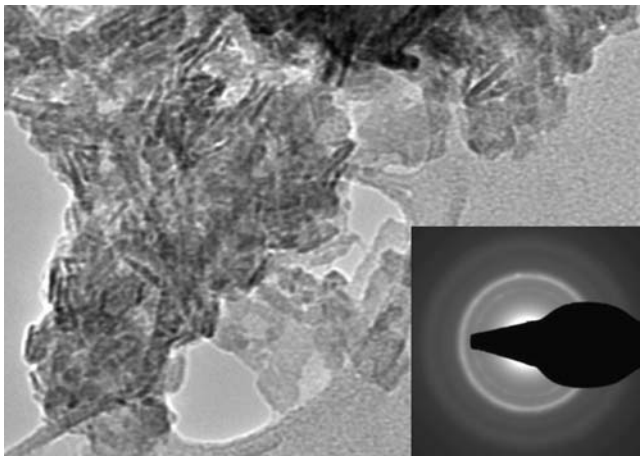

Fig. 1 Transmission electron microscopic (TEM) images of bone at a high magnification and in the *insert* an electron diffractogram. Distinct individual HAP crystals are observed displaying needle-like morphologies

The presence of carbonate groups

Special attention has to be paid to the presence of molecular groups such $(CO_3)^{2-}$ at the surface or inside the crystal. Such molecular entities play a key role in the formation and evolution, the physical properties and on the morphology of apatite. For example, Kapolos et al. [19] put forward that carbonate incorporated on the seed crystals caused changes in their morphology, favouring plate-like formations.

From a chemical point of view, carbonate apatite [see for example the early works of Santos et al. [20] and Elliott et al. [21] can form through a substitution for either the hydroxyl group (A type) or the phosphate group (B type). Several investigations indicate that type B carbonate is the major species in biological apatites. This is in line with the research of Astala et al. [22] dedicated to carbonate substitution mechanisms in bulk hydroxyapatite. Their results confirm that B (or PO_4) site substitutions are energetically preferred to A (or OH^-) site substitutions.

For type A carbonated apatite, the substitution of a monovalent anion by a divalent one is compensated by the creation of a vacancy and the chemical composition can be represented by:

$$Ca_{10}(PO_4)_6CO_3\square$$

where ❑ represents the vacancy. This representation is in fact far too simple. At this point, we have to consider the spatial repartition of the atoms. Since apatite structure is quite well known (i.e. the space group is $P6_3/m$, the values for the crystallographic parameters are $a=b=9.41844$ Å, $c=6.88374$ Å and the position of the different atoms are gathered in Table 1), we can represent their spatial arrangement at the nanometre scale (Fig. 2). We can see

Table 1 Atomic coordinates for hydroxyapatite $Ca_{10}(PO_4)_6(OH)_2$

Atoms	*x*	*y*	*z*
Ca [I]	1/3	2/3	0.0016
Ca [II]	0.246	0.9923	0.25
P	0.398	0.368	0.25
O1	0.3275	0.4841	0.25
O2	0.5869	0.4649	0.2500
O3	0.3436	0.258	0.0705
O	0.00	0.00	0.1975
H	0.000	0.000	0.054

easily hydrogen and oxygen atoms of the hydroxyl groups (in blue) located on the *c*-axis.

As proposed by Suetsugu et al. [23], for the position of CO_3^{2-} ions (replacing the OH^- group) six possibilities around the *c*-axis are in fact possible for a same chemical composition. In Fig. 3, the triangles represent CO_3^{2-} with one of three C–O bonds of CO_3^{2-} laying on the *c*-axis. From an energetic point of view, the existence of pattern (e) or (f) is implausible. Moreover, these authors noticed that the substitution of CO_3^{2-} ion in the A site is accompanied by compression of PO_4^{3-} tetrahedron along the *c*-axis.

Regarding type B carbonated apatite, the substitution of a PO_4^{3-} group by a CO_3^{2-} mainly causes the creation of a Ca^{2+} vacancy and an OH^- vacancy. These compounds can be thus represented by:

$$Ca_{10-x+u}\square_{x-u}(PO_4)_{6-x}(CO_3)_xOH_{2-x+2u}\square_{x-2u}$$

with $0<x<2$ and $0<u<x$.

Now if we take into account the spatial arrangement of the atoms in HAP, calcium atoms are associated with two different positions namely Ca[I] and Ca[II] (Table 1). Thus, from a structural point of view, the precise position of the vacancy regarding Ca has to be determined [24].

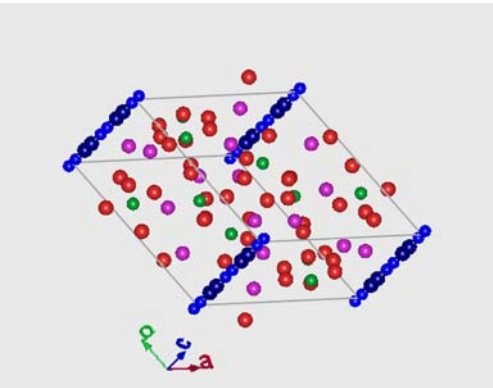

Fig. 2 Spatial repartition of the different atoms in the case of HAP. Hydrogen and oxygen atoms of the hydroxyl groups represented in *blue* are located on the *c*-axis

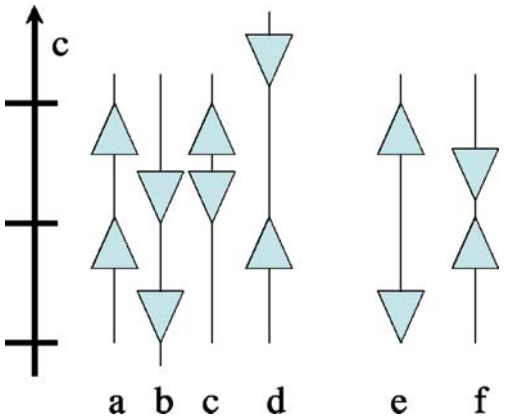

Fig. 3 Combination patterns of CO_3–CO_3 pair in the A site. *Triangles* represent CO_3^{2-} with one of three C–O bonds of CO_3 laying on the *c*-axis. Note that existence of pattern (e) or (f) is implausible

The presence of oligoelements

Different oligoelements, namely Mg, Fe, Sr, Se and Zn, play a key role in several essential biological functions. Recently, we classify these trace elements present in pathological calcifications and we underline in the case of apatite-based kidney stones a substitution process with Ca [25].

In the case of physiological calcifications, significant efforts have been done to understand the mechanism of fixation of these oligoelements at the surface of apatites [26–28]. Among them, Sheha et al. [29] have reported that the sorption of Zn (II) increases with increasing pH value. It seems in fact that the mechanism of metals interaction with apatite is intimately dependent on the experimental conditions, i.e. pH and the nature of the Zn(II) species for example.

Also, several works underlined the influence of small amounts of cations on the reactivity and stability of natural bioapatites, inducing subtle changes in their microstructural features. More precisely, through high resolution electronic microscopy, Cuisinier et al. [30] have noticed that the incorporation of Zn^{2+} cations in the crystal lattice of the carbonate-containing apatite reduces the number of structural defects.

The interface between the apatite and the biological environment

An added refinement to such structural description is achieved in studies of the interface between the nanocrystals of apatite and the biological environment. This interface plays a significant role in the growth of the calcification. As pointed out by Rey et al. [31, 32], an exciting characteristic of apatite is the existence of a structured surface hydrated layer which is at the core of protein/inorganic recognition and interaction [33, 34]. Also, this structured surface hydrated layer can be considered as the precursor of HAP.

At this point, we have thus to introduce octacalcium phosphate (OCP, $Ca_8H_2(PO_4)_6$, $5H_2O$) considered by many authors as the most probable precursor of HAP in in vivo studies. Recently, Tseng et al. [35] have gained valuable insight into the molecular mechanism of OCP to HAP transformation. Using a scanning electron microscope (SEM) and TEM, they follow the transformation of blade-like OCP crystals into hexagonal rod-shaped HAP crystals as the pH of the reaction mixture increases slowly from 4.35 to 6.69 in 12 h.

It is important also to underline that some oligoelements have an effect in the phase transformation between calcium phosphate compounds. For example, Lundager-Madsen [36] has recently pointed out a marked effect of cations on the transformation from brushite ($CaHPO_4$, $2H_2O$) to OCP and HAP. While Cu and Zn are strong inhibitors, Pb seems to be a moderate promoter.

As a preliminary conclusion of this presentation, the set of studies we have selected here show clearly that a fine description of structural characteristics of the nanocrystals of HAP including their size and their orientation is crucial to establish a significant relationship with mechanical properties of bone. Nevertheless, such characterisation at the nanometre scale of the mineral part of bone is not sufficient. We have also to pay attention to carbonate groups as well as to oligoelements present at the surface of the apatite nanocrystals. Obviously, when appropriate, information regarding the organic part of bones, i.e. collagen fibrils has to be collected.

The diffraction techniques

X-ray and neutron scattering techniques have emerged to be two of the most powerful tools in material science [37]. Each atom of the sample defines a scattered wave built from an incident beam made either of photons, neutrons or electrons. The uniform spatial configuration of atoms causes the interference pattern of each wave. This interference pattern is measured through a collection of diffraction peaks, their positions and their intensities being intimately related to the spatial arrangement of the atoms.

Diffraction techniques can be used either to determine the crystal structure [38, 39] or the chemical composition of the samples through the powder diffraction bank data file [40] which contains more than 64,000 patterns. Regarding nanometre-scale materials, numerous academic and industrial laboratories have pursued research of such nanometre-scale entities [41]. This research has profited from an increasing experimental effort, leading to elegant experiments aimed at characterising and understanding several physical–chemical processes playing an important role in physics, chemistry and in biology.

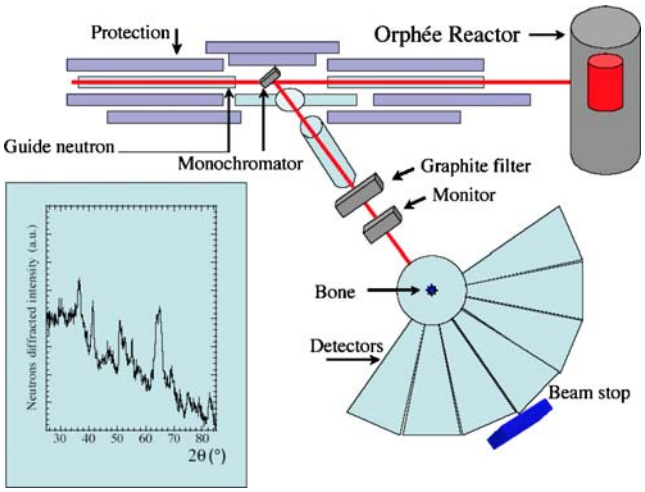

Fig. 4 Schematic view of an experimental setup of a diffraction beamline. In the *insert*, a typical neutron diffraction diagram of a bone made of nanocrystals of apatite is visualised

An example of beamline dedicated to PND and implemented on a neutron source is the G 4-1 beamline (http://www-llb.cea.fr/spectros/pdf/g41-llb.pdf). This experimental device (Fig. 4) is composed of a two-axis powder diffractometer equipped with a vertical focusing pyrolytic graphite monochromator and an 800-cell multidetector covering an 80°–2θ range (step 0.1° between two cells). In our experiments, part of bones without crushing has been studied. Also, recent experimental developments lead to real-time in situ observations as well as experiments on microsamples.

Diffraction techniques yield some essential information regarding the size, the strain, the morphology and the orientation of the nanocrystals. Broadening of the diffraction peaks is the result of two physical factors namely size and microstrain and we can evaluate their effect separately [42]. Nanometre scale of crystals yield diffraction peaks which are broadened because the fewer the atomic planes that give rise to Bragg diffraction, the less sharp is the peak. A quantitative analysis based on the Scherrer equation links the broadening of the diffraction peak to the size of the nanocrystals.

Regarding the orientation of the nanocrystals, Bacon and Goodship [43] have shown through neutron diffraction that the long bones of animals have the *c*-axes of their apatite crystals preferentially oriented to withstand stresses. Recent experimental developments combining a monochromatic X-ray beam (<30 μm) with a charge-coupled device camera allow a relatively easy quantification of crystal alignment in bone tissue [44].

Neutron versus X-ray scattering

Neutrons as a probe at the atomic scale provide a set of non-destructive investigation techniques. Their complemen-

tarity with synchrotron radiation may be illustrated through two physical parameters related to the fraction of the sample which is analysed as well as the amplitude of the interaction between the probe and the matter. The first one is the penetration depth of the probe while the atomic diffusion factor defines the second one.

Since neutrons are electrically neutral, they interact only weakly with matter into which they can penetrate deeply. Thus, structural information given by PND corresponds to the bulk. PND gives the opportunity to establish an intimate relationship between the average size of nanocrystals which compose bones and some particular features defined at the macroscopic scale. In addition, synchrotron radiation (SR) diffraction takes advantage of its short penetration depth (around 20 μm) as well as of the small size of the beam to establish a structural mapping of the biological entity at the micrometre scale.

Regarding the second parameter, the atomic diffusion factor, it explains why the differences (between X-ray and neutrons) in positional parameters for heavy atoms are marginal but are crucial for light atoms especially for hydrogen atoms [45]. Thus, in some case, it is more appropriate to select neutron scattering than X-ray scattering [46]. For example, in order to explain the higher bioactivity of the silicon-substituted hydroxyapatite (SiHA), Arcos et al. [47, 48] have considered neutron diffraction. The enhanced bioactivity of SiHA versus synthetic ceramic HAP is correlated to higher thermal displacement parameters of H atoms.

Finally, note that in neutron-diffraction measurements of the orientation of apatite crystals, for studying the stress distribution in bone, it is necessary to remove substantially the collagen in order to reduce the incoherent scattering [49]. That is why Cedola et al. [50] performed high spatial resolution small-angle X-ray scattering (SAXS) measurements using SR [51–53]. They used the fact that the collagen D-period (≅67 nm) along the fibril axis produces SAXS peaks to show that the collagen distribution roughly follows the mineralisation distribution. Also, Almer and Stock [54] have reported the first simultaneous quantification of Young's modulus in the separate material phases of bone (fibril of collagen and nanocrystals of hydroxyapatite). This advance in diffraction studies of bones represents a milestone since they follow at the same time the strain in the mineral (WAXS) and in the collagen phases (SAXS) as a function of applied load.

Synthetic and biological apatites

In order to discuss some specific aspects regarding biological apatites, we have plotted in Fig. 5 the neutron diffraction diagrams of three families of apatites. High-temperature-calcinated stoichiometric hydroxyapatite gives very fine diffraction peaks in line with the fact that such

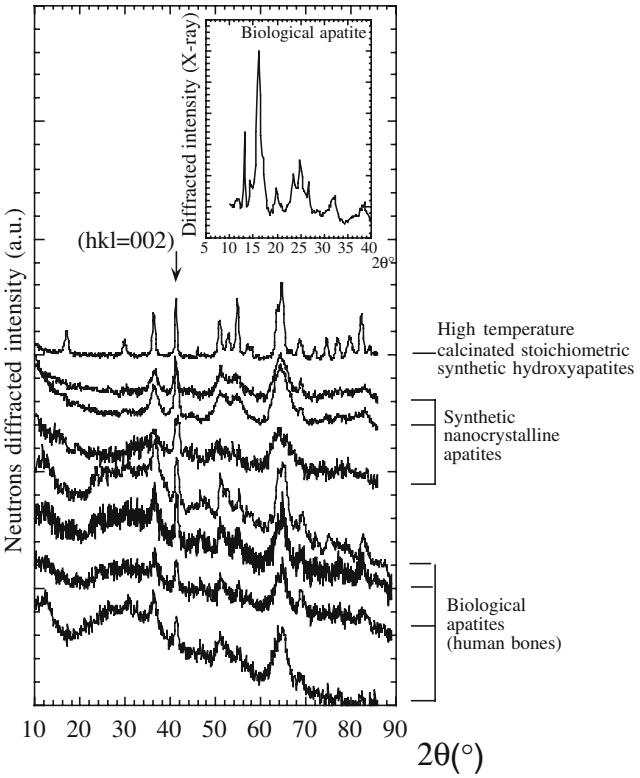

Fig. 5 Neutron diffraction diagrams of three families of apatite: high-temperature-calcinated synthetic apatite, room-temperature synthetic apatites and biological apatites (bones). In the *insert*, an X-ray diffraction diagram is visualised

materials are made of large nanocrystals (their dimension is around 200 nm). At the opposite, the diffraction peaks related to non-stoichiometric nanocrystalline apatites which are synthesised at room temperature as well as to the ones related to biological apatites (here bones) are very large. For these materials, the size is typical around 10 nm. Moreover, for all these apatites (synthesised at room temperature and biological ones), the width of a diffraction peak (hkl=002) is smaller than the width of the other diffraction peaks, pointing out the anisotropy of the nanocrystals of all these compounds (needle and/or platelet-like morphology).

It is important to underline that a broad study including X-ray diffraction data of apatites of different biological origins indicates that the nanometre size as well as the anisotropy of the nanocrystals are often observed. It seems that these structural characteristics of apatite are dominated by the chemistry and thus be considered as an intrinsic property.

Finally, we have to introduce the fact that in the case of neutron diffraction, due to the large value of the penetration depth, all the atoms of the sample contribute to the diffraction diagram. We take full advantage of this parameter by considering the incoherent signal coming

from hydrogen atoms, i.e. a signal without diffraction peak and proportional to the number of hydrogen atoms. This specificity of neutrons (for x-ray and electrons, hydrogen atoms are quite invisible) leads to the fact that it is possible to point out the presence of an amorphous phase and evaluate its proportion in a sample including a crystalline phase. In that case, special standards and particular experimental conditions are required.

Considering substitution processes

Diffraction techniques offer the possibility to consider substitution processes. For example, carbonate substitutions in apatites are known to change the crystal lattice parameters. Pure type A substitution (CO_3^{2-} for OH^-) causes expansion of the crystallographic parameter *a* and the contraction of the crystallographic parameter *c* [55]. In contrast, pure type B carbonated apatite (CO_3^{2-} for PO_4^{3-}) causes contraction of *a* and expansion of *c* parameters.

Regarding the replacement of Ca^{2+} cations by other cations, numerous studies have been performed in order to locate the foreign cations in the HAP structure. Among them, let us quote Mg [56], Si [57], Cd [58], Sr [59] and Pb [60]. More precisely, Zhu et al. [61] founded that the metal ions of Pb^{2+}, Sr^{2+} and Cd^{2+} preferentially occupied Ca[II] sites in the apatite structure (two occupation sites exist as gathered in Table 1) . Similar results were obtained recently by Tamm et al. [62]. The authors indicate that the bigger ions occupied the Ca[II] sites preferentially since in site Ca [II], the arrangement of the staggered equilateral triangles allows for the optimisation of the packing of large ions while in Ca[I] the strict alignment in the columns causes a stronger repulsion. Thus, metal ions with bigger ionic radius or electronegativity preferentially occupy the Ca[II] sites. Note that this occupancy depends on the concentration of the oligoelements. The structure refinements obtained by Bigi et al. [63] indicate that whilst in most of the range of concentration strontium displays a slight preference for the Ca[II] site coherently with its ionic radius, at very low concentrations its occupancy of the smaller Ca[I] site is slightly higher.

X-ray absorption spectroscopy

We should recognise that due to the low content of oligoelements inside bones, diffraction techniques have to be completed by a structural investigation through X-ray absorption spectroscopy (XAS) [64]. XAS gathers the X-ray absorption near edge structure (XANES) and extended X-ray absorption fine structure (EXAFS) techniques (Fig. 6). Basically, photons with sufficient energy, i.e. above a characteristic energy called the absorption threshold E_0, are able to extract an electron from the core. This

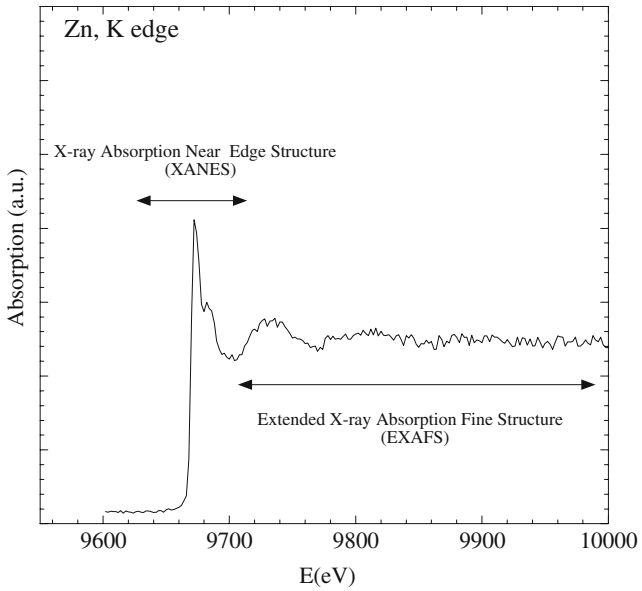

Fig. 6 X-ray absorption spectra including the XANES and the EXAFS collected at the Zn K edge for a bone specimen

electron or "photoelectron" is the probe associated with this spectroscopy. If the energy of the photon (*E*) is near the absorption threshold E_0 (E_0-100 eV$<E<E_0+40$ eV), information regarding the electronic state [65] of the photoexcited atoms is available (XANES). A higher *E* value (E_0+40 eV$<E<E_0+1{,}500$ eV) is indicative of the arrangement of the atoms around the photoexcited atoms.

First, the local environment of Ca has been investigated in bones [66–69]. Special attention has been paid to amorphous calcium phosphate [70–73] such compounds given very poor structured diffraction diagrams. Note that the conversion process between amorphous calcium phosphate into HAP has been also studied [74].

EXAFS studies have been also performed to determine the environment of other cations such Ga [75], Pb [76] or Cd [77] in order to locate these cations inside the mineral. In the case of Sr, its incorporation in several calcium phosphate compounds including apatitic tricalcium phosphate, HAP, OCP and dicalcium phosphate dihydrate have been considered [78].

More precisely regarding HAP, the analysis of EXAFS experiments [75] leads to an environment of Sr atoms composed by six oxygen atoms at a distance of 2.54 Å and 2.4 oxygen atoms at 2.70 Å. The obtained Sr–O distances were slightly longer than those determined by X-ray crystallography for Ca coordination in HAP, e.g. 2.54 versus 2.38 Å in line with the work of Kay et al. [79].

Recently, we have performed a set of X-ray absorption experiments [80] using DIFFABS, a beamline implemented on SOLEIL (Source Optimisée de Lumière d'Energie Intermédiaire du LURE), the new French synchrotron facility (St Aubin). This experimental setup offers the possibility of studying the short- and medium-range

structural characteristics of materials by the almost simultaneous combination of XAS and WAXS.

Several biological apatites (bones) as well as a commercial HAP used as a reference compound have been selected for this investigation. The content of Sr in all these apatites (biologic and synthetic) is similar to the content of other biological apatites, i.e. between 400 and 500 ppm. As we can see in Fig. 7, the XANES part of the absorption spectra is quite similar, indicating for all these samples an electronic state 2+ for the strontium atoms. In Fig. 8 is plotted a function giving the spatial repartition of atoms around strontium. This function is obtained through a Fourier transform of the EXAFS modulations situated after the Sr K edge. Strontium atoms are positioned at R=0Å and thus the first peak just before 2Å (feature a in Fig. 8) is dominated by the presence of oxygen atoms. Then, the peak around 3Å (feature b in Fig. 8) is due to atoms situated around Sr atoms at larger distances. As we can see, the commercial HAP is associated with a more intense (b) peak in line with the fact that apatite nanocrystals are larger for this sample. Even if the quantitative analysis is currently in progress, a first qualitative analysis seems to indicate that Sr atoms have the same environment for all the samples considered here.

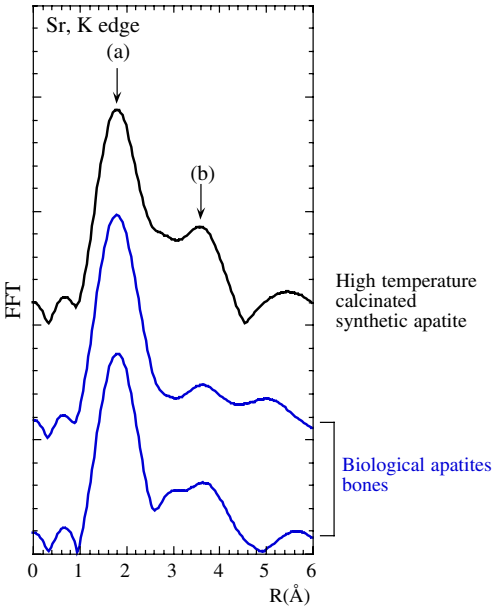

Fig. 8 Fourier transforms of the EXAFS oscillations situated after the Sr K edge of different bones and of a high-temperature-calcinated synthetic apatite

Raman spectroscopy

Raman scattering, discovered in 1928 [81] is a very useful practical way of studying molecular groups inside or at the surface of apatite. The physical process associated with it is as follows: an incident beam at a frequency ω_0 interacts with molecules. Emergent beams (detected perpendicular to the incident beam) with different frequencies are measured. In most cases, the initial state is the ground state and thus the scattered photon (or Stokes) has lower energy than the exciting photon. At the opposite, for the small fraction of the molecules in vibrationally excited states, the scattered photon appears at higher energy (or 'anti-Stokes'). The difference between the Stoke (or anti-Stokes) frequency and the initial frequency $\omega_S - \omega_0$ (or $\omega_{AS} - \omega_0$) is intimately related to the vibrational spectra of the molecules. It is thus possible to identify the different molecules present inside the sample and the intensity of the signal can be used to determine their concentration.

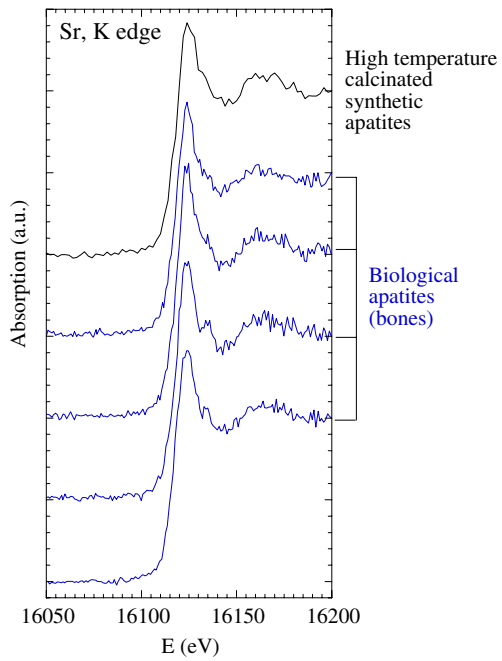

Fig. 7 XANES part of the absorption spectra near the Sr K edge for different bones compared to the XANES collected for a high-temperature-calcinated synthetic apatite

From an experimental point of view, the intensity relative to the frequencies $\omega_S - \omega_0$ or $\omega_{AS} - \omega_0$ is quite small, i.e. only 1 in 10^7 of the incident photon gives rise to a Raman signal. This experimental fact explains why this technique has undergone a resurgence as a result of the use of lasers (green, red or near-infrared lasers).

Several variations of Raman spectroscopy [82] have been developed in order to enhance the sensitivity or improve the spatial resolution. While the initial wavelength is usually below the first electronic transitions of most molecules, a subtle modification of the basic Raman effect arrives when the incident beam has the frequency of an electron transition of the molecule. Such particular value for the initial frequency ω_0 confers a higher sensitivity (in that case the intensity of some Raman-active vibrations

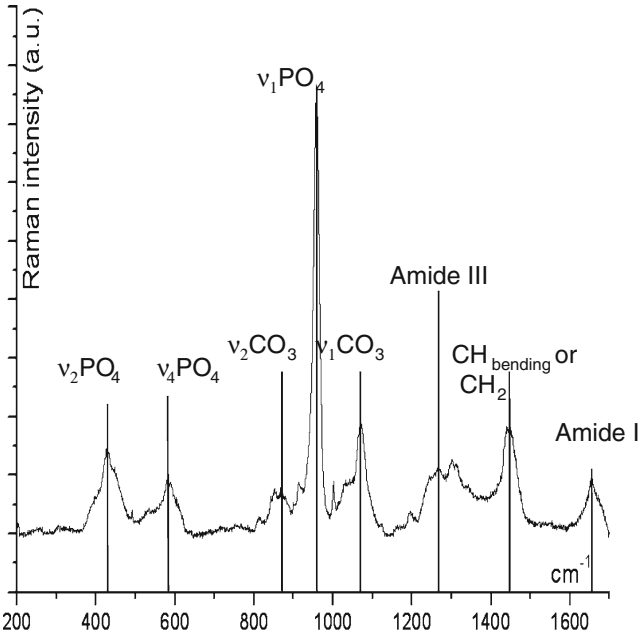

Fig. 9 Typical Raman spectra of bones, contributions of PO_4^{3-} and CO_3^{2-} are pointed out

increases by a factor of 10^2–10^4) and a drastic simplification of the Raman signal (only a few number of vibrational modes are excited). This configuration conducts the scientific community to replace in the case of a particular application the laser by synchrotron radiation [83]. Similar improvements regarding the sensitivity of Raman spectroscopy may be obtained through coherent anti-Stokes Raman spectroscopy using two lasers [84]. This technique known as CARS, acronym for coherent anti-Stokes Raman scattering, constitutes also a significant improvement in terms of sensitivity (around 10^6 versus conventional Raman spectroscopy). Finally, regarding the spatial resolution, coupling Raman spectroscopy to atomic force microscopy device leads to nanometre probes (see for example [85]).

Raman spectroscopy has been widely applied to the study of mineralised tissues [83, 86, 87]. The review paper, written by Boskey et al. [88], depicts different major breakthroughs based on microspectroscopy (infrared and Raman) including the detection of diseases and drug-induced modifications. Part of this success is due to the fact that the chemistry of calcium phosphate is quite complex and that slight variation of Raman bands among different calcium phosphate compounds exists [89].

Measurement of disorder through Raman spectroscopy

As noticed by Morris and Carden [90], a typical Raman spectrum of bone is complex (Fig. 9). First, a large peak at 960 cm^{-1} is measured corresponding to the totally symmetric ν_1 stretch of PO_4^{3-}. These authors stated that this particular feature constitutes an interesting indicator of the degree of crystallinity. At 955 cm^{-1}, this structure is associated with an amorphous highly carbonated bone while at 963 cm^{-1} it corresponds to a more ordered non-carbonated bone. The degree of crystallinity is thus related to the carbonate level, an experimental fact already examined by Penel et al. [91]. These authors give several major insights to such correlation. At first, they indicate that the variations of $\nu_1PO_4^{3-}$ band half-width observed for a set of type B apatites (4.5%, 7% and 10 wt.% carbonate) are significant (equal to 13, 15 and 17 cm^{-1}, respectively). Then, they report that the high values of $\nu_1PO_4^{3-}$ band half-width (20 and 18 cm^{-1}) measured for dentine and bone compared to the one obtained for enamel (14 cm^{-1}) is in line with the lower carbonate level content and higher crystallinity of enamel.

As a beginning of explanation of this intimate correlation between Raman and disorder, we can just recall that the local environment of the PO_4 molecular groups are affected by several structural characteristics related to:

- the presence of carbonate (apatites containing around 6% carbonate correspond to the substitution of one PO_4^{3-} in the unit cell by a CO_3^{2-})
- the existence of vacancies and/or oligoelements
- the small size of the crystals

The carbonate substitution

Different publications use the fact that types A and B ν_1 carbonate bands can be detected separately, at 1,103 and 1,071 cm^{-1}, respectively (Fig. 9). At this point, it can be interesting to note that similar measurements through FT-IR (Fig. 10) lead to the same characteristics. A-type and B-

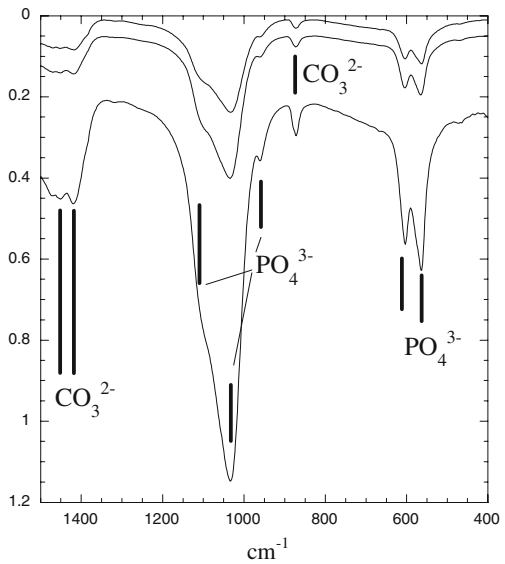

Fig. 10 FT-IR spectra of bones, contributions of PO_4^{3-} and CO_3^{2-} are pointed out

type carbonate can be respectively monitored by the 878 and 872 cm^{-1} components of $\nu_2CO_3^{2-}$. Interestingly, a feature at 866 cm^{-1} is associated with supplementary species of carbonate, i.e. a labile carbonate [92].

Recently, Awonusi et al. [93] have prepared a series of apatites with varying carbonate levels in order to calibrate the Raman signals. Such calibration is of primary importance as illustrated by the following CO_3/ν_2PO_4 ratio in interstitial and osteonal bone tissue regions. Following the same approach, Timlin et al. [94] point out that differences in mineral composition are seen near the rim of an osteon and further out in the lamellae.

Study of microcracks and relationship with pathology

Sahar et al. [95] review the current understanding of damage mechanisms derived from a set of techniques including Raman spectroscopy as well as laser confocal microscopy, SEM and TEM. Timlin et al. [96] noticed that in the region of visible microdamage, an unusually high-frequency component to the phosphate ν_1 band (963 cm^{-1}), corresponding to a more stoichiometric mineral species, appears in the region of microcracks. Note that such high-frequency component was not seen in undamaged areas. It is thus quite clear that these experiments provide evidence that compositional changes are associated with regions of damage.

Interface with biological environment

Raman spectroscopy offers the possibility to study not only the mineral part of the sample through the vibration of the PO_4^{3-} group but also the organic part. The collagen fibrils are visualised through the amide I (at 1,660 cm^{-1}), the methylene (CH_2 at 1,450 cm^{-1}) and the amide III (at 1,260 cm^{-1}). Such opportunity leads to an evaluation of the amount of mineralisation indicating through ν_2PO_4/amide III ratio as well as the fibre orientation given by ν_1PO_4/amide I ratio.

Several exciting results have been also obtained by McCreadie et al. [97]. In their study, they observed that for fractured women, the femoral trabecular bone is associated with a higher carbonate/amide I area ratio compared to the one measured for unfractured women. Other interesting results have been obtained for iliac crest biopsies. The complete set of data revealed a higher carbonate/phosphate ratio in cortical bone from women who had sustained a fracture.

Conclusion

The literature on diffraction techniques and vibrational spectroscopy is quite large and only a restricted number of investigations have been presented. Crucial information regarding the organic and inorganic parts of bone is available. In fact, modern studies combine several techniques [98, 99]. For example, diffraction diagrams and vibrational data can be collected at the same time using photons from a synchrotron radiation centre as a probe. Regarding bones, recent experimental devices have been developed in order to mimic the stress and due to the heterogeneity of the sample, acquisition data can be performed through mapping at the micrometre scale. Thus, major breakthroughs in many areas of the medical science are on their way.

Acknowledgements The authors thank Dr. A. Canizares and Dr. P. Simon regarding Raman spectra and the staff of SOLEIL. This work was supported by the Physics and Chemical Departments of the CNRS.

Conflicts of interest None.

References

1. Currey JD (2005) Hiearchies in biomineral structures. Science 309:253
2. Mann S (1993) Molecular tectonics in biomineralization and biomimetic materials chemistry. Nature 365:499–505
3. Elliott JC (2002) Calcium phosphate biominerals. In: Kohn MJ, Rakovan J, Hughes JM (eds) Phosphates: geochemical, geobiological and materials importance, reviews in mineralogy and geochemistry, vol 48. Mineral Society of America, Washington DC, pp 427–453
4. Elliott JC (1994) Structure and chemistry of the apatites and other calcium orthophosphates. Elsevier, Amsterdam
5. Guinier A (1956) X-ray diffraction in crystals, imperfect crystals and amorphous bodies. Dunod, Paris
6. Kneipp K, Kneipp H, Itzkan I, Dasari RR, Feld MS (1999) Ultrasensitive chemical analysis by Raman spectroscopy. Chem Rev 99:2957–2975
7. McKelvy ML, Britt TR, Davis BL, Gillie JK, Graves FB, Lentz LA (1998) Infrared spectroscopy. Anal Chem 70:119–177
8. Bertsch PM, Hunter DB (2001) Applications of synchrotron-based X-ray microprobes. Chem Rev 101:1809–1842
9. Dumas P, Sockalingum GD, Sule-Suso J (2006) Adding synchrotron radiation to infrared microspectroscopy: what's new in biomedical applications? Trends Biotechnol 25:40–44
10. Bazin D, Guczi L, Lynch J (2002) Anomalous wide angle X-ray scattering (AWAXS) and heterogeneous catalysis. Appl Catal 226:87–113
11. Gouadec G, Ph Colomban (2007) Raman Spectroscopy of nanomaterials: how spectra relate to disorder, particle size and mechanical properties. Prog Cryst Growth Charact Mater 53:1–56
12. Naray-Szabo S (1930) The structure of apatite (CaF)Ca4(PO4)3. Z. Kristallogr Kristallgeom Kristallphys Kristallchem 75:387–398
13. White TJ, Zhi Li D (2003) Structural derivation and crystal chemistry of apatites. Acta Crystallogr B 59:1–16
14. Rey C, Miquel JL, Facchini L, Legrand AP, Glimcher MJ (1995) Hydroxyl groups in bone mineral. Bone 16:583–586
15. Loong CK, Rey C, Kuhn LT, Combes C, Wu Y, Chen SH, Glimcher MJ (2000) Evidence of hydroxyl-ion deficiency in bone apatites: an inelastic neutron-scattering study. Bone 26:599–602
16. Cho G, Wu Y, Ackerman JL (2003) Detection of hydroxyl ions in bone mineral by solid state NMR spectroscopy. Science 300:1123–1127
17. Vallet-Regı M, Gonzalez-Calbet MJ (2004) Calcium phosphates as substitution of bone tissues. Prog Solid State Chem 32:1–31

18. Grynpas MD, Holmyard D (1988) Changes in quality of bone mineral on aging and in disease. Scanning Microsc 2:1045–1054
19. Kapolos J, Koutsoukos PG (1999) Formation of calcium phosphates in aqueous solutions in the presence of carbonate ions. Langmuir 15:6557–6562
20. Santos M, Gonzalez-Diaz PF (1977) A model for B carbonate apatite. Inorg Chem 16:2131–2134
21. Elliott JC, Bonel G, Trombe JC (1980) Space group and lattice constants of Ca10 (PO4) 6CO3. J Appl Crystallogr 13:618–621
22. Astala R, Stott MJ (2005) First principles investigation of mineral component of bone: CO_3 substitutions in hydroxyapatite. Chem Mater 17:4125–4133
23. Suetsugu Y, Takahashi Y, Okamura FP, Tanaka J (2000) Structure analysis of a-type carbonate apatite by a single-crystal X-ray diffraction method. J Solid State Chem 155:292–297
24. Wilson RM, Elliott JC, Dowker SEP, Rodriguez-Lorenzo LM (2005) Rietveld refinements and spectroscopic studies of the Ca-deficient apatite. Biomaterials 26:1317–1327
25. Bazin D, Chevallier P, Matzen G, Jungers P, Daudon M (2007) Heavy elements in urinary stones. Urol Res 35:179–184
26. Xu Y, Shawartz FW, Traina SJ (1994) Sorption of Zn^{2+} and Cd^{2+} on hydroxyapatite surfaces. Environ Sci Technol 28:1472–1480
27. Lusvardi G, Menabue L, Saladini M (2002) Reactivity of biological and synthetic HAP towards Zn(II) ion, solid–liquid investigations. J Mater Sci Mater Med 13:91–98
28. Cheung CW, Porter JF, MacKay G (2002) Removal of Cu(II) and Zn(II) ions by sorption onto bone char using batch agitation. Langmuir 18:650–656
29. Sheha RR (2007) Sorption behavior of Zn(II) ions on synthesized hydroxyapatites. J Colloif Interface Sci 310:18–26
30. Cuisinier FJG, Steuer P, Voegel JC, Apfelbaum F, Mayer I (1995) Structural analyses of carbonate-containing apatite samples related to mineralized tissues. J Mater Sci Mater Med 6:85–89
31. Rey C, Combes C, Drouet C, Sfihi H, Barroug A (2007) Physico-chemical properties of nanocrystalline apatites: implications for biominerals and biomaterials. Materials Science and Engineering C 27:198–205
32. Cazalbou S, Eichert D, Drouet C, Combes C, Rey C (2004) Minéralisations biologiques à base de phosphate de calcium. C. R. Pale 3:563–572
33. Wang L, Guan X, Du C, Moradian-Oldak J, Nancollas GH (2007) Amelogenin promotes the formation of elongated apatite microstructures in a controlled crystallization system. J Phys Chem C 111:6398–6404
34. Seeman NC, Belcher AM (2002) Emulating biology: building nanostructures from the bottom up. Proc Natl Acad Sci U S A 99:6452–6455
35. Tseng YH, Mou CY, Chan JCC (2006) Solid-state NMR study of the transformation of octacalcium phosphate to hydroxyapatite: a mechanistic model for central dark line formation. J Am Chem Soc 128:6909–6918
36. Lundager-Madsen HE (2008) Influence of foreign metal ions on crystal growth and morphology of brushite and its transformation to octacalcium phosphate and apatite. J Cryst Growth 310:2602–2612
37. Warren BE (1990) X-ray diffraction. Dover, New York
38. Rietveld HM (1969) A profile refinement method for nuclear and magnetic structure. J Appl Crystallogr 2:65–71
39. Le Bail A, Loüer D (1978) Smoothing and validity of crystallite size distributions from X-ray line profile analysis. J Appl Crystallogr 11:50–55
40. Powder diffraction file (PDF), International Centre for Diffraction Data, 12 campus Blvd, Newton square, PA 19073-3273, USA, http://www.idd.com.
41. Bazin DC, Sayers DA, Rehr JJ (1997) Comparison between X-ray absorption spectroscopy, anomalous wide angle X-ray scattering, anomalous small angle X-ray scattering, and diffraction anomalous fine structure techniques applied to nanometer scale metallic clusters. J Phys Chem B 101:11040–11050
42. Klug H, Alexander L (1974) X-ray diffraction procedures for polycrystalline and amorphous materials, 2nd ed. Wiley, New York
43. Bacon GE, Goodship AE (2007) The healing process for fractured tibia bones of sheep studied by neutron diffraction. J Appl Crystallogr 40:349–353
44. Heidelbach F, Riekel C, Wenk HR (1999) Quantitative texture analysis of small domains with synchrotron radiation X-rays. J Appl Crystallogr 32:841–849
45. Hamilton WC (1969) Comparison of X-ray and Neutron diffraction structural results: A study in methods of error analysis. Acta Crystallogr A 25:194–206
46. Wilson RM, Elliott JC, Dowker SEP, Smith RI (2004) Rietveld structure refinement of precipitated carbonate apatite using neutron diffraction data. Biomaterials 25:2205–2213
47. Arcos D, Rodríguez-Carvajal J, Vallet-Regí M (2004) Neutron scattering for the study of improved bone implants. Phys Rev B Condens Matter 350:E607–E610
48. Arcos D, Rodríguez-Carvajal J, Vallet-Regí M (2004) The effect of the silicon incorporation on the hydroxylapatite structure. A neutron diffraction study. Solid State Sc 6:987–994
49. Bacon GE, Bacon PJ, Griffiths RK (1979) The orientation of apatite crystals in bone. J Appl Crystallogr 12:99–103
50. Cedola A, Mastrogiacomo M, Lagomarsino S, Cancedda R, Giannini C, Guagliardi A, Ladisa M, Burghammer M, Rustichelli F, Komlev V (2007) Orientation of mineral crystals by collagen fibers during in vivo bone engineering: an X-ray diffraction imaging study. Spectrochim Acta B 62:642–647
51. Zhou H, Burger C, Sics I, Hsiao BS, Chu B, Graham B, Glimcher MJ (2007) Small angle X-ray study of the three-dimensional collagen/mineral superstructure in intramuscular fish bone. J Appl Crystallogr 40:666–668
52. Gupta S, Roschger P, Zizak I, Fratzl-Zelman N, Nader A, Klaushofer K, Fratzl P (2003) Mineralized microstructure of calcified avian tendons: a scanning small angle X-ray scattering study. Calcif Tissue Int 72:567–576
53. Gupta HS, Wagermaier W, Zickler GA, Hartmann J, Funari SS, Roschger P, Wagner HD, Fratzl P (2006) Fibrillar level fracture in bone beyond the yield point. Int J Fract 139:425–436
54. Almer JD, Stock SR (2005) Micromechanical response of mineral and collagen phases in bone. J Struct Biol 152:14–27
55. DeMaeyer E, Verbeeck R, Nassens D (1993) Stoichiometry of Na+ and CO_3^{2-} containing apatites obtained by hydrolysis of monetite. Inorg Chem 32:5709–5714
56. Bigi A, Falini G, Foresti E, Gazzano M, Ripamonti A, Roveri N (1996) Rietveld structure refinements of calcium hydroxyapatite containing magnesium. Acta Crystallogr B 52:87–92
57. Tian T, Jiang D, Zhang J, Lin Q (2008) Synthesis of Si-substituted hydroxyapatite by a wet mechanochemical method. Mat Sci Eng C28:57–63
58. Marchat D, Bernache-Assolant D, Champion E (2007) Cadmium fixation by synthetic hydroxyapatite in aqueous solution—thermal behavior. J Hazard Mater A139:453–460
59. Landi E, Sprio S, Sandri M, Celotti G, Tampieri A (2008) Development of Sr and CO_3^{2-} co-substituted hydroxyapatites for biomedical applications. Acta Biomater 4:656–663
60. Laperche V, Traina SJ, Gaddam P, Logan TJ (1996) Chemical and mineralogical characterizations of Pb in a contaminated soil: reactions with synthetic apatite. Environ Sci Technol 30:3321–3326
61. Zhu K, Yanagisawa K, Shimanouchi R, Onda A, Kajiyoshi K (2006) Hydrothermal synthesis and crystallographic study of Sr Pb HAP solid solutions. J Eur Ceram Soc 26:509–513

62. Tamm T, Peld M (2006) Computational study of cation substitutions in apatites. J Solid State Chem 179:1581–1587
63. Bigi A, Boanini E, Capuccini C, Gazzano M (2007) Sr-substituted HAP nanocrystals. Inorg Chim Acta 360:1009–1016
64. Sayers DA, Lytle FW, Stern EA (1970) In: Henke BL, Newkirk JB, Mallett GR (eds) Advances in X-ray analysis, vol 13. Plenum, New York, pp 248-271
65. Bazin D, Rehr JJ (2003) Limits and advantages of XANES for nanometer scale metallic clusters. J Phys Chem B 107:12398–12402
66. Harries JE, Hukins DWL, Hasnain SS (1988) Calcium environment in bone mineral determined by EXAFS spectroscopy. Calcif Tissue Int 43:250–253
67. Harries JE, Hasnain SS, Shah JS (1987) EXAFS study of structural disorder in carbonate-containing hydroxyapatites. Calcif Tissue Int 41:346–350
68. Eichert D, Salomé M, Banu M, Susini J, Rey C (2005) Preliminary characterization of calcium chemical environment in apatitic and non-apatitic calcium phosphates of biological interest by XAS. Spectrochim Acta B 60:850–858
69. Liou SC, Chen SY, Lee HY, Bow JS (2004) Structural characterization of nanosized calcium deficient apatite powders. Biomaterials 25:189–196
70. Eanes ED, Powers L, Costa JL (1981) EXAFS studies on calcium in crystalline and amorphous solids of biological interest. Cell Calcium 2:251–262
71. Miller RM, Hukins DWL, Hasnain SS, Lagarde P (1981) EXAFS studies of the calcium ion environment in bone mineral and related calcium phosphates. Biochem Biophys Res Com 99:102–106
72. Holt C, Van Kemenade MJJM, Nelson LS, Hukins DWL, Bailey RT, Harries JE, Hasnain SS, DeBruyn PL (1989) Amorphous calcium phosphate prepared at pH6 and 6.5. Mater Res Bull 24:55–62
73. Nelson LS, Holt C, Harries JE, Hukins DWL (1989) Amorphous calcium phosphates of different composition give very similar EXAFS spectra. Physica B 158:105–106
74. Harries JE, Hukins DWL, Holt C, Hasnain SS (1987) Conversion of amorphous calcium phosphate into HAP investigated by EXAFS spectroscopy. J Cryst Growth 84:563–570
75. Korbas M, Rotika E, Meyer-Klaucke W, Ryczek J (2004) Bone tissue incorporates in vitro gallium with a local structure similar to gallium-doped brushite. J Biol Inorg Chem 9:67–76
76. Sugiyama S, Moriga T, Hayashi H, Moffat JB (2001) Characterization of Ca, Sr, Ba and Pb HAP: X-ray diffraction, photoelectron, EXAFS and MAS NMR spectroscopies. Bull Chem Soc Jpn 74:187–192
77. Sery A, Manceau A, Greaves GN (1996) Chemical state of Cd in apatite phosphate ores as determined by EXAFS spectroscopy. Am Mineral 81:864–873
78. Rokita E, Hermes C, Nolting HF, Ryczek J (1993) Substitution of calcium by Sr within selected calcium phosphates. J Cryst Growth 130:543–552
79. Kay MI, Young RA, Posner AS (1964) Crystal structure of HAP. Nature 204:1050–1052
80. Bazin D, Carpentier X, Traxer O, Thiaudière D, Somogyi A, Reguer A, Waychunas G, Jungers P, Daudon M (2008) Very first tests on SOLEIL regarding the Zn environment in pathological calcifications made of apatite determined by X-ray absorption spectroscopy. J Synchrotron Radiat 15((Pt 5):506–509
81. Raman CV, Krishnan KS (1928) A new radiation. Indian J Phys 2:387–398
82. Kudelski A (2008) Analytical applications of Raman spectroscopy. Talanta 76(1):1–8
83. Prince KC, Kuepper K, Neumann M, Cooco D, Bondino F, Zangrando M, Zacchigna M, Mateeucci M, Parmigiani F (2004) Resonant Raman X-ray scattering at the S2p edge of iron pyrite. J Phys Condens Matter 16:7397–7404
84. Zumbusch A, Holtom GR, Xie XS (1999) Vibrational microscopy using coherent anti-Stokes Raman scattering. Phys Rev Lett 82:4142–4145
85. Habelitz S, Marshall GW, Balooch M, Marshall SJ (2002) Nanoindentation and storage of teeth. J Biomech 35:995–998
86. Carden A, Rajachar RM, Morris MD, Kohn DH (2004) Ultrastructure changes accompanying the mechanical deformation of bone tissues: a Raman imaging study. Calcif Tissue Int 72:166–175
87. Balooch M, Habelitz S, Kinney JH, Marshall SJ, Marshall GW (2008) J Struct Biol 162(3):404–410
88. Boskey AL, Mendelsohn R (2005) Infrared spectroscopic characterization of mineralized tissues. Vibr Spectrosc 38:107–114
89. Numata Y, Sakae T, Suwa T, Nakada H, Legeros RZ, Kobayashi K (2008) Qualitative and quantitative evaluation of bone and synthetic calcium phosphates using Raman spectroscopy. Key Eng Mater 361–363:135–138
90. Morris MD, Carden A, Rajachar RM, Kohn DH (2002) Effects of applied load on bone tissue as observed by Raman spectroscopy. Proc SPIE 4614:47–54
91. Penel G, Leroy G, Rey C, Bres C (1998) MicroRaman spectral study of the PO_4 and CO_3 vibrational modes in synthetic and biological apatites. Calcif Tissue Int 63:475–481
92. Rey C, Collins B, Goehl T, Dickson RI, Glimcher MJ (1989) The carbonate environment in bone mineral. A resolution enhanced Fourier transform infrared spectroscopy study. Calcif Tissue Int 45:157–164
93. Awonusi A, Morris MD, Tecklenburg MJM (2007) Carbonate assignment and calibration in the Raman spectrum of apatite. Calcif Tissue Int 81:46–52
94. Timlin JA, Carden A, Morris MD (1999) Chemical microstructure of cortical bone probed by Raman transects. Appl Spectrosc 53:1429–1435
95. Sahar ND, Hong SI, Kohn DH (2005) Micro- and nano-structural analyses of damage in bone. Micron 36:617–629
96. Timlin JA, Carden A, Morris MD, Rajachar RM, Kohn DH (2000) Raman spectroscopic markers for fatigue-related bovine bone microdamage. Anal Chem 72:2229–2236
97. McCreadie BR, Morris MD, Chen TC, Rao DS, Finney WF, Widjaja E, Goldstein SA (2006) Bone tissue compositional differences in women with and without osteoporotic fracture. Bone 39:1190–1195
98. Daudon M, Bazin D, Jungers P, André G, Cousson A, Chevallier P, Véron E, Matzen G (2009) Opportunities offered by scanning electron microscopy, powder neutron diffraction and synchrotron radiation mX-ray fluorescence in the study of whewellite kidney stones. J App Cryst 42:109–115
99. Bazin D, Daudon M, Chevallier P, Rouzière S, Elkaim E, Thiaudière D, Fayard B, Foy E, Albouy PA, André G, Matzen G, Veron E (2006) Les techniques de rayonnement synchrotron au service de la caractérisation d'objets biologiques : un exemple d'application, les calculs rénaux. Annales de Biologie Clinique 64 (2):125–139